A measure from line-of-sight magnetograms for prediction of coronal mass ejections

D. A. Falconer,[1] R. L. Moore, and G. A. Gary
Marshall Space Flight Center, Huntsville, Alabama, USA

Received 9 May 2003; revised 2 July 2003; accepted 23 July 2003; published 29 October 2003.

[1] From a sample of 17 vector magnetograms of 12 bipolar active regions we have recently found (1) that a measure of the overall nonpotentiality (the overall twist and shear in the magnetic field) of an active region is given by the strong shear length L_{SS}, the length of the portion of the main neutral line on which the observed transverse fields is strong (>150 Guass (G)) and strongly sheared (shear angle >45°), and (2) that L_{SS} is well correlated with the coronal mass ejection (CME) productivity of the active regions during the ±2-day time window centered on the day of the magnetogram. In the present paper, from the same sample of 17 vector magnetograms, we show that there is a viable proxy for L_{SS} that can be measured from a line-of-sight magnetogram. This proxy is the strong gradient length L_{SG}, the length of the portion of the main neutral line on which the potential transverse field is strong (>150 G), and the gradient of the line-of-sight field is sufficiently steep (greater than ~50 G/Mm). In our sample of active regions, L_{SG} is statistically significantly correlated with L_{SS} (correlation confidence level >95%), and L_{SG} is as strongly correlated with active region CME productivity as is L_{SS} (correlation confidence level ~99.7%). Because L_{SG} can be measured from line-of-sight magnetograms obtained from conventional magnetographs, such as the magnetograph mode of the Michelson Doppler Imager (MDI) on board the Solar and Heliospheric Observatory, it is a dependable substitute for L_{SS} for use in operational CME forecasting. In addition, via measurement of L_{SG}, the years-long, nearly continuous sequence of 1.5-hour cadence full disk line-of-sight magnetograms from MDI can be used to track the growth and decay of the large-scale nonpotentiality in active regions and to examine the role of this evolution in active region CME productivity. *INDEX TERMS:* 7513 Solar Physics, Astrophysics, and Astronomy: Coronal mass ejections; 7524 Solar Physics, Astrophysics, and Astronomy: Magnetic fields; 2118 Interplanetary Physics: Energetic particles, solar; 2788 Magnetospheric Physics: Storms and substorms; *KEYWORDS:* coronal mass ejection, prediction, halo, space weather, flare, active region

Citation: Falconer, D. A., R. L. Moore, and G. A. Gary, A measure from line-of-sight magnetograms for prediction of coronal mass ejections, *J. Geophys. Res.*, *108*(A10), 1380, doi:10.1029/2003JA010030, 2003.

1. Introduction

[2] Every large, fast (supersonic) coronal mass ejection (CME) erupts from a region of closed magnetic field on the Sun [*Webb*, 1992]. The stronger of these CME-producing magnetic explosions are usually seated in regions of strong field, namely large active regions with sunspots, and produce a region-spanning flare in tandem with the CME [*Rust et al.*, 1980; *MacQueen and Fisher*, 1983; *Moore*, 1988; *Moore et al.*, 1999]. The fast CME drives hazardous space weather in the form of intense solar energetic particle events and severe geomagnetic storms [*Suess and Tsurutani*, 1998; *Reames*, 2001]. Development of methods for predicting these CME explosions is important both for the practical benefit of improved forecasting of damaging space weather and because it is a way to test and improve our physical understanding of these and similar magnetic explosions on the Sun and in many other astrophysical settings. This paper presents a measure of an active region's magnetic structure that gauges whether the active region is likely to be CME-productive, and that can be measured from a line-of-sight magnetogram.

[3] To be able to explode, an active region's magnetic field must contain free magnetic energy. That is, the field must be in a stressed, deformed configuration relative to the minimum-energy potential field configuration that it would have if it were completely relaxed and had no stored energy. From observations of the magnetic structure of active regions, it is known that bipolar active regions that produce CMEs typically have an overall nonpotential field configuration of a characteristic form [*Moore and LaBonte*, 1980; *Canfield et al.*, 1999; *Moore et al.*, 1997, 2001]. In chromospheric images and photospheric vector magnetograms the signature of this configuration is strong magnetic

[1] Also at University of Alabama in Huntsville, Huntsville, Alabama, USA.

0148-0227/03/2003JA010030$09.00

shear along the active region's main neutral line, the neutral line of the overall bipolar field of the active region [*Moore et al.*, 1987; *Falconer et al.*, 2002]. That is, in the core of the bipole the field rooted near the neutral line is directed nearly along the neutral line, nearly orthogonal to the direction of the potential field. In coronal images, such as the soft X-ray images from Yohkoh, the signature is sigmoidal magnetic structure illuminated by enhanced coronal heating [*Canfield et al.*, 1999; *Falconer*, 2001]. This structure has the overall shape of either an "S" or an inverse S, and the middle of the S traces the sheared core field through the active region. Combined with photospheric magnetograms, the sigmoidal coronal structure shows that the whole bipolar field has an overall twist, that the core field is greatly sheared, and that shear and the twist are in the same sense (right-handed for S shape and left-handed for inverse S shape). Often there is a chromospheric filament suspended in the sheared core field. In a CME explosion, this filament usually erupts as an integral part of the core of the CME [*Rust et al.*, 1980; *Moore*, 2001], indicating that the CME is driven by explosion of the highly nonpotential sheared core field [*Moore*, 1988; *Moore et al.*, 2001]. Moreover, *Canfield et al.* [1999] found that active regions that show obvious overall sigmoidal structure in coronal images are more CME productive than are active regions that have no recognizable sigmoidal structure. Thus strong large-scale nonpotentiality of this form in an active region's magnetic field is a favorable condition for a CME explosion.

[4] The above observations suggest that an active region's CME productivity depends strongly on the active region's degree of overall nonpotentiality. Below some low level of nonpotentiality a CME explosion should not be possible, whereas at high enough levels of nonpotentiality a CME explosion should be nearly certain. On this basis it is reasonable to expect that some quantitative measure of active region nonpotentiality might prove to be a good predictor of active region CME productivity.

[5] To explore this approach to CME prediction, in our recent work [*Falconer*, 2001; *Falconer et al.*, 2002], we adopted three measures of active region nonpotentiality that can be measured from a vector magnetogram, measured these quantities in a sample of active regions, and examined their correlation with the CME productivity of the active regions. We limited these initial studies to predominantly bipolar active regions because sigmoidal active regions are typically bipolar overall and because each of our three measures is most simply interpreted as a measure of the overall magnetic shear and/or twist in a bipolar active region. Our three measures are (1) L_{SS}, the length of strong magnetic shear along the main neutral line, (2) I_N, the net electric current in the bipole, and (3) α, the magnetic twist parameter given by the net current normalized by the total magnetic flux (Φ) in the active region ($\alpha = \mu I_N/\Phi$, where μ is the permeability of free space). L_{SS} is easier to measure than are I_N or α, because, of the three, only L_{SS} can be measured without resolving the 180° ambiguity in the direction of the transverse field in a vector magnetogram. In the work of *Falconer et al.* [2002], from 17 vector magnetograms of 12 active regions, we found that these three nonpotentiality measures were all well correlated with each other and that all three were about equally well correlated with the CME productivity of the active regions during the time intervals spanning 2 days before and after the day of each magnetogram (correlation confidence level ~99%). Each of the three measures was also significantly correlated with the CME productivity of active region in time intervals spanning 4 days before and after the day of each magnetogram (correlation confidence level ≥96%).

[6] Thus it appears that any of these three measures of active region nonpotentiality would be useful in operational CME forecasting (for either Earthward CMEs or west-limb CMEs [*Falconer et al.*, 2002]), if the measure could be routinely provided at least once per day for each active region on the central face of the Sun (within a few days of rotation from central meridian). For this use, L_{SS} probably would be the best of the three because L_{SS} is the easiest to measure, and, unless a larger sample of active regions proves otherwise, L_{SS} is practically as well correlated with active region CME productivity as are I_N or α. In addition, L_{SS} is more readily generalized to yield a measure of the overall nonpotentiality of active regions that are magnetically more complex than bipolar active regions. (Many CME-productive active regions are multibipolar, i.e., are composed of two or more impacted bipoles [*Machado et al.*, 1988; *Moore et al.*, 1999; *Aulanier et al.*, 2000; *Sterling and Moore*, 2001]). The generalized L_{SS} is simply the total length of all intervals of strong magnetic shear on all neutral lines in an active region [*Falconer*, 1997].

[7] Even though L_{SS} is easier to obtain than I_N or α, it does require a vector magnetogram of the active region and hence requires the use of a vector magnetograph, which measures both the component of the field vector along the line of sight and the rest of the vector, the component transverse to the line of sight. A conventional magnetograph measures only the line-of-sight component of the magnetic field. Relative to vector magnetographs, conventional magnetographs are simpler, more robust, and more proven for monitoring solar magnetic fields continuously and uniformly over many years. The Michelson Doppler Imager (MDI) [*Scherrer et al.*, 1995], presently in operation on board the Solar and Heliospheric Observatory (SOHO), produces full-disk line-of-sight magnetograms, usually at a cadence of 16 per day, and has done so nearly continuously and with little degradation since 1996. NASA's Solar Dynamics Observatory (SDO) [*Hathaway et al.*, 2001], planned for launch in 2007, is to have a full disk magnetograph that will provide line-of-sight magnetograms with better sensitivity, cadence, and resolution than MDI. Only if resources allow, will the SDO magnetograph be made capable of making vector magnetograms. So, for operational CME forecasting, it is desirable to have a measure of active region nonpotentiality that can be obtained from a line-of-sight magnetogram and that is as well correlated with active region CME productivity as is L_{SS}.

[8] It is well known that for active region neutral lines across which the gradient of the line-of-sight field ($\nabla B_{\|}$) is very large, such as in delta sunspots, the core field along the neutral line is nearly always very strongly sheared [*Moore and Rabin*, 1985; *Zirin and Liggett*, 1987; *Zirin*, 1988]. In the set of 17 vector magnetograms that we used by *Falconer et al.* [2002], a correlation of neutral line magnetic gradient with neutral line magnetic shear is noticeable from visual inspection of the vector magnetograms. This suggests that the length of main neutral line strong shear, L_{SS}, is correlated

Table 1. Measured Magnetic Quantities L_{SS} and L_{SG} and Number of Observed CME Events in Our Active Regions[a]

AR	Date of Magnetogram	L_{SS}, 10^3 km[b]	L_{SG}, 10^3 km[c]	Number of CMEs[d]
6982	26 Dec. 1991	97 ± 20*	81 ± 17*	1
7070	27 Feb. 1992	84 ± 17*	72 ± 15*	1
7070	28 Feb. 1992	78 ± 16*	90 ± 19*	1
7220	12 July 1992	18 ± 6	36 ± 8*	0
7260	16 Aug. 1992	39 ± 9	35 ± 8	0
7315	19 Oct. 1992	2 ± 5	0 ± 5	0
7315	21 Oct. 1992	5 ± 5	0 ± 5	0
7315	23 Oct. 1992	30 ± 8	35 ± 8	0
7999	27 Nov. 1996	34 ± 8	0 ± 5	0
8083	7 Sept. 1997	13 ± 5	0 ± 5	0
8100	31 Oct. 1997	20 ± 6	5 ± 5	0
8100	3 Nov. 1997	62 ± 13*	42 ± 10*	2
8108	18 Nov. 1997	23 ± 7	35 ± 8	2
8323	2 Sept. 1998	74 ± 16*	11 ± 5	0
9026	6 June 2000	106 ± 22*	38 ± 9*	2
9077	14 July 2000	158 ± 32*	91 ± 19*	2
9077	16 July 2000	130 ± 26*	71 ± 15*	1

[a]L_{SS}, strong shear length; L_{SG}, strong gradient length; AR, active region; CME, coronal mass ejection. Asterisks denote measured values that are greater than or equal to the threshold value at and above which the active region is expected to be CME productive in the ±2-day window and below which the active region is expected to not be CME productive in the ±2-day window.

[b]Length of main neutral line on which observed $B_\perp$ >150 G and shear angle >45°. Threshold length is 62,000 km.

[c]Length of main neutral line on which potential $B_\perp$ >150 G and observed $|\nabla B_{||}|$ >50 G/Mm. Threshold length is 36,000 km.

[d]Number of CME events identified in the active region within ±2 days from the day of the magnetogram.

with a length, L_{SG}, the length of the main neutral line segment on which $\nabla B_{||}$ is above some selected threshold value. If for some threshold in $\nabla B_{||}$, L_{SG} were correlated well enough with L_{SS}, L_{SG} would effectively be a measure of active region nonpotentiality that could be used in CME forecasting.

[9] In this paper, we use the active regions, magnetograms, and CME counts from *Falconer et al.* [2002] to explore the correlation of L_{SG} with L_{SS} and with CME productivity. For a $\nabla B_{||}$ threshold of 50 Guass per mega meter (G/Mm) we find that L_{SG} is a promising measure of active region nonpotentiality for CME prediction; in this sample of active regions L_{SG} is well correlated with L_{SS} and is as strongly correlated with CME productivity as is L_{SS}.

2. Data and Analysis Procedure

[10] The active region magnetograms used in this study are the 17 vector magnetograms used by *Falconer et al.* [2002]. They are all from the Marshall Space Flight Center (MSFC) vector magnetograph [*Hagyard et al.*, 1982; *West et al.*, 2002] and sample 12 active regions. Each magnetogram is of one active region on some day when the active region was viewed more or less face-on (was no farther than 30° from central meridian). Each magnetogram was selected by this criterion and by the criterion that the active region be basically bipolar, i.e., have an obvious main neutral line. The active regions and the dates of their magnetograms are listed in Table 1. The vector magnetogram for one of the more CME-productive active regions is shown in Figure 1. This vector magnetogram displays a typical concurrence of strong gradient in the line-of-sight field and strong magnetic shear along the main neutral line.

[11] For each magnetogram, the number of CMEs produced by the active region in the ±2-day time window centered on the day of the magnetogram was determined as described by *Falconer et al.* [2002] from Yohkoh coronal X-ray images in combination with soft X-ray flux time profiles from GOES and CME observations from the Large Angle Spectrometric Coronagraph (LASCO) on SOHO. In Table 1, we have listed for each magnetogram the observed number of CMEs produced by the active region during the 5-day time interval. See *Falconer et al.* [2002] for discussion of uncertainties due to misidentified or missed CMEs.

[12] The strong shear length L_{SS} and the strong gradient length L_{SG} are measured from each magnetogram. The method of measuring L_{SS} is as described by *Falconer* [2001] and *Falconer et al.* [2002]. The method of measuring L_{SG} is basically the same method applied to a line-of-sight

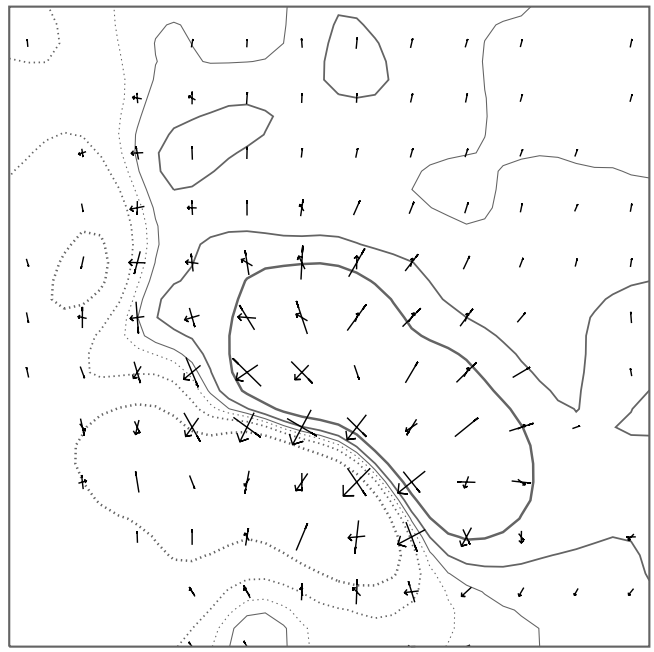

Figure 1. Marshall Space Flight Center vector magnetogram of active region 9026 on 6 June 2000, with computed potential transverse field vectors superposed. The field of view is 110 × 110 arc sec, north up, west right. The line-of-sight component of the magnetic field is mapped by the contours; the thicker the contour the stronger the field (25 G, 100 G, 250 G; solid contours for positive polarity and dotted contours for negative polarity). The strength and direction of the observed transverse field are mapped by the dashes (the shortest for 150 G and the longest for strengths ≥500 G). For clarity the transverse field is plotted for only one in nine pixels. The arrows map the strength and direction of the potential transverse field computed from the observed line-of-sight field. The greater the shear in the magnetic field, the greater the shear angle; the shear angle is the acute angle between the observed and potential transverse fields. This coronal mass ejection (CME) productive, predominantly bipolar, active region is typical in that strong magnetic shear and steep gradient in the line-of-sight field are both concentrated along the main polarity dividing line.

magnetogram rather than a vector magnetogram. We will first review the method of measuring L_{SS} and then describe the analogous method for measuring L_{SG}.

[13] To measure L_{SS}, the first step is to compute the transverse component of the potential field from the line-of-sight component of the vector magnetogram and overlay it on the vector magnetogram, as in Figure 1 [*Falconer et al.*, 1997]. The next step is to identify the strong field segments of the main neutral line, the segments on which the observed transverse fields has strength above some threshold. The field strength threshold that we use is 150 G, which strength is twice the noise level in the transverse component of the MSFC vector magnetograms [*Gary et al.*, 1987]. This choice ensures that the uncertainty in the measured shear angle, the acute angle between the observed and potential transverse field, is less than $\sim 10°$ everywhere on the strong field main neutral line. The strong shear length L_{SS} is the total length of the strong shear parts of the strong field main neutral line, the parts on which the shear angle is above some large threshold. We use 45° for the threshold of strong magnetic shear. For the active region vector magnetogram shown in Figure 1, the strong field portion of the main neutral line is shown in the first panel of Figure 2. In this example, the shear angle is >45° along the entire length of the strong field neutral line.

[14] To measure L_{SG}, the first step is again to compute the transverse potential field from the line-of-sight component of the vector magnetogram but then combine this with only the line-of-sight component of the magnetogram, as if we had no vector magnetogram but only a conventional line-of-sight magnetogram. The strong field segments of the main neutral line are then defined as those segments on which the potential transverse field strength is above some threshold, which we again choose to be 150 G. For our example magnetogram of Figure 1, the main neutral line's strong field portion found in this way is shown in Figure 2 (right). It is somewhat longer than the strong field interval found from the full vector magnetogram and shown in the first panel of Figure 2. The strong gradient length L_{SG} is the total length of the strong gradient part of this redefined strong field main neutral line, the parts on which the gradient $|\nabla B_{\|}|$ is above some threshold. We will find that a useful L_{SG} is given by any gradient threshold within a factor of two of 50 G/Mm. Figure 2 (right) shows that in this example active region $|\nabla B_{\|}|$ is >50 G/Mm along only about half or less of the strong field main neutral line.

[15] In Table 1, measured values of L_{SS} and L_{SG} are listed for each magnetogram. The L_{SG} values are for a strong gradient threshold of 50 G/Mm. The uncertainty in each measured value of L_{SS} or L_{SG} is the square root of the sum of the squares of two uncertainties, from two separate sources of error [*Falconer*, 2001]. One source of error is the polarization sensitivity of the vector magnetograph, which gives root-mean-square noise of 50 G in the line-of-sight component of the vector magnetogram and 75 G in the transverse component [*Gary et al.*, 1987]. This noise gives the lengths L_{SS} and L_{SG} each an uncertainty of ~ 2 pixel widths, which is $\sim 5 \times 10^3$ km. The other source of error is the blurring of the magnetogram by the seeing conditions at the observatory. For average seeing conditions, this results in an uncertainty of $\sim 20\%$ in L_{SS} and L_{SG} [*Falconer*, 2001].

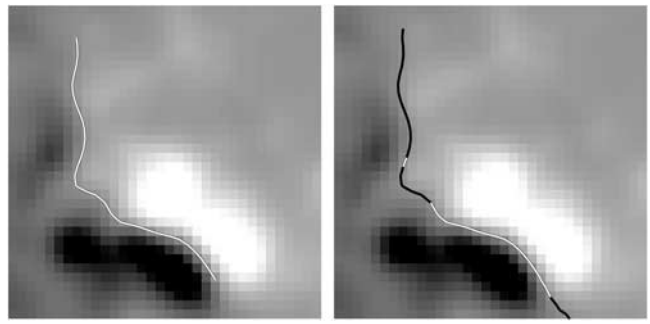

Figure 2. Strong shear length (L_{SS}) and strong gradient length (L_{SG}) in the example active region of Figure 1. In both panels of Figure 2 the shaded background image is the line-of-sight field (lighter shading for positive polarity and darker shading for negative polarity). The open line (left) marks the extent of the main neutral line on which the observed transverse field is stronger than 150 G. All of this part of the main neural line is shown open, indicating that in this active region the shear angle exceeded 45° everywhere on this strong field part of the main neutral line. The strong shear length L_{SS} is the length of this open part of the main neutral line. The solid and open line (right) marks the extent of the main neutral line on which the potential transverse field (but not necessarily the observed transverse field) is stronger than 150 G. On the open parts the gradient of the line-of-sight field exceeds 50 G/Mm; on the solid parts the gradient is below this threshold. The strong gradient length L_{SG} is the total length of these open parts of the main neutral line.

[16] Inspection of Table 1 shows that in our sample of active regions (1) the active regions having the larger values of L_{SS} tend to also have the larger values of L_{SG} and (2) the active regions that were CME productive tend to have larger values of L_{SS} and L_{SG} than do the active regions that were not CME productive. We evaluate the statistical significance of these correlations by basically the same method that we used previously [*Falconer et al.*, 2002]. The first step is to adopt threshold values of L_{SS} and L_{SG}, at and above which we expect an active region to produce at least one CME during the ±2-day window and below which we expect it to produce no CMEs in this interval. For each of our measures, L_{SS} and L_{SG}, we take this threshold value to be the percentile value corresponding to the fraction of active region vector magnetograms for which the active region did produce one or more CMEs in the ±2-day window. For our set of 17 vector magnetograms, 8 are of active regions that were CME-productive in the ±2-day window. Hence for threshold values of L_{SS} and L_{SG} we take the eighth largest of the 17 measured values of each. We thus assign a threshold value of 62,000 km for the strong shear length L_{SS} and threshold value of 36,000 km for the strong gradient length L_{SG}.

[17] From the L_{SS} and L_{SG} threshold values for CME expectation, we then obtain, for the set of 17 pairs of measured values (L_{SS}, L_{SG}) in Table 1, a 2×2 contingency table for whether or not the magnetograms have both lengths above threshold or both below threshold (as in Table 2). From each threshold, each set of 17 values of L_{SS} or L_{SG}, and the set of 17 CME counts we obtain another

Table 2. Correlation of L_{SG} With L_{SS}

Defining Condition for L_{SG}	Contingency Condition	L_{SS} < Threshold	$L_{SS} \geq$ Threshold	Confidence Level	Success Rate
$\|\nabla B_{\|\|}\|$ > 25 G/Mm	$L_{SG} \geq$ Threshold	2	6	95.6%	76%
	L_{SG} < Threshold	7	2		
$\|\nabla B_{\|\|}\|$ > 50 G/Mm	$L_{SG} \geq$ Threshold	1	7	99.7%	88%
	L_{SG} < Threshold	8	1		
$\|\nabla B_{\|\|}\|$ > 100 G/Mm	$L_{SG} \geq$ Threshold	1	7	99.7%	88%
	L_{SG} < Threshold	8	1		

2×2 contingency table for whether CMEs were or were not produced in the ±2-day window when the measured length was above or below threshold (as in Table 3). The degree of correlation in each case (L_{SG} with L_{SS}, L_{SS} with CME productivity, and L_{SG} with CME productivity) is determined from the corresponding contingency table by the Fisher test, which gives the confidence level of the correlation in terms of a percentage [*Everitt*, 1977; *Falconer et al.*, 2002]. This percentage is $(1 - P) \times 100\%$, where P is the probability that a correlation (i.e., inequality in the population of the four quadrants of the contingency table) as great as or greater than the observed correlation would occur by random chance. A confidence level of $\geq$95% is conventionally considered to be statistically significant [*Everitt*, 1977].

3. Results

[18] The middle panel of Figure 3 is the correlation plot of the measured values of L_{SS} and L_{SG} listed in Table 1, the L_{SG} values being those for a $|\nabla B_{\|}|$ threshold of 50 G/Mm. The left panel of Figure 3 is the correlation plot for the L_{SG} values found from a twice-smaller $|\nabla B_{\|}|$ threshold (25 G/Mm), and the right panel is the plot for a twice-larger threshold (100 G/Mm). In each of the three panels of Figure 3 the 17 values of L_{SS} are the same, and the vertical line marks the L_{SS} threshold (62,000 km) at and above which CME production is expected. The horizontal line in each panel of Figure 3 marks the L_{SG} CME expectation threshold for the set of 17 L_{SG} values found from the given $|\nabla B_{\|}|$ threshold. Relative to the L_{SG} threshold (36,000 km) for the case of $|\nabla B_{\|}|$ >50 G/Mm (middle panel of Figure 3), the L_{SG} threshold for $|\nabla B_{\|}|$ >25 G/Mm (left panel of Figure 3) is ~2 times longer, and the L_{SG} threshold for $|\nabla B_{\|}|$ > 100 G/Mm (right panel of Figure 3) is ~6 times shorter. The L_{SG} threshold decreases with increasing $|\nabla B_{\|}|$ threshold because the length of L_{SG} in each magnetogram decreases with increasing $|\nabla B_{\|}|$ threshold. The points plotted below $L_{SG} = 2 \times 10^3$ km in Figure 3 are for magnetograms in which no part of the main neutral line has $|\nabla B_{\|}|$ above threshold, resulting in $L_{SG} = 0$. For $|\nabla B_{\|}|$ >25 G/Mm, only 1 of the 17 magnetograms has magnetic gradient below this threshold everywhere on its strong field main neutral line (left panel of Figure 3). Doubling the $|\nabla B_{\|}|$ threshold to 50 G/Mm resulted in L_{SG} dropping to zero in three more magnetograms (middle panel of Figure 3), and doubling the threshold again to 100 G/Mm decreased L_{SG} to zero in an additional five magnetograms (right panel of Figure 3).

[19] In each panel of Figure 3, the L_{SS} and L_{SG} threshold lines delineate the four quadrants that define the corresponding 2×2 contingency table in Table 2. For each of the three sets of L_{SG} values the confidence level and success rate of the correlation of L_{SG} with L_{SS} are given in Table 2 and in the upper right corner of the correlation plot in Figure 3. In the case of the first panel in six magnetograms, L_{SG} and L_{SS} are both at or above threshold, in seven magnetograms, L_{SG} and L_{SS} are both below threshold, in two magnetograms, L_{SG} is above threshold but L_{SS} is below threshold, and in the remaining two magnetograms, L_{SG} is below threshold but L_{SS} is at or above threshold. This distribution gives a correlation confidence level of 95.6% and a success rate of 76% (13 successes out of 17 trials). In each of the second and third panels, 15 of the 17 points are in the two ''agreement'' quadrants and only 2 points are in the two ''disagreement'' quadrants. This reduction in the failure rate from 4 out of 17 to 2 out of 17 increases the correlation confidence level to 99.7% (0.3% probability of occurring by chance) and increases the success rate to 88% (15/17). Thus in our sample of 17 vector magnetograms, for $|\nabla B_{\|}|$ thresholds in the vicinity of 50 G/Mm, L_{SG} is statistically significantly correlated with L_{SS} (confidence level >95%).

[20] In each panel of Figure 3, 8 of the 17 (L_{SG}, L_{SS}) points are marked by asterisks, and the other 9 points are

Table 3. Correlation of L_{SS} and L_{SG} With Active Region CME Productivity

	Contingency Condition	Not CME Productive	CME Productive	Confidence Level	Success Rate
Defining	$L_{SS} \geq$ Threshold	1	7	99.7%	88%
Condition for L_{SG}	L_{SS} < Threshold	8	1		
$\|\nabla B_{\|\|}\|$ > 25 G/Mm	$L_{SG} \geq$ Threshold	2	6	95.6%	76%
	L_{SG} < Threshold	7	2		
$\|\nabla B_{\|\|}\|$ > 50 G/Mm	$L_{SG} \geq$ Threshold	1	7	99.7%	88%
	L_{SG} < Threshold	8	1		
$\|\nabla B_{\|\|}\|$ > 100 G/Mm	$L_{SG} \geq$ Threshold	0	8	99.996%	100%
	L_{SG} < Threshold	9	0		

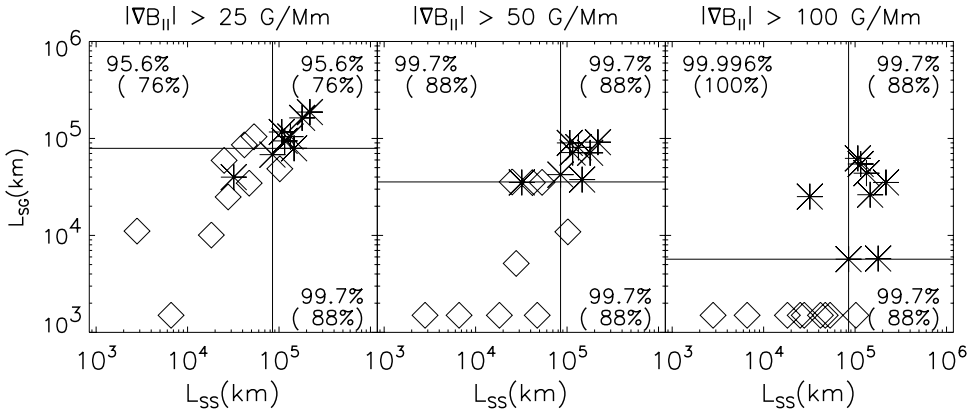

Figure 3. Correlation plots of values of L_{SS} and L_{SG} measured in our 17 magnetograms. In each panel of Figure 3 the L_{SS} values of the 17 points are those listed in Table 1. Each L_{SG} value (left) is the extent of the strong field main neutral line having line-of-sight field gradient steeper than 25 G/Mm. The L_{SG} values (middle) are for a line-of-sight field gradient threshold of 50 G/Mm and are those listed in Table 1. The L_{SG} values (right) are for a threshold of 100 G/Mm. The vertical line in each panel of Figure 3 marks the L_{SS} threshold value at and above which the active region is expected to be CME productive in the ±2-day window. The threshold value of L_{SG} for CME expectation is marked by the horizontal line in each panel of Figure 3. The points for magnetograms of CME-productive active regions are marked by asterisks; the points for magnetograms of non-CME-productive active regions are marked by diamonds. The two percentages in the upper right corner of each panel of Figure 3 are the confidence level and success rate of the correlation of L_{SG} with L_{SS} (from Table 2); those in the lower right corners are for the correlation of L_{SS} with CME productivity (from Table 3); those in the upper left corners are for the correlation of L_{SG} with CME productivity (from Table 3).

marked by diamonds. The asterisks in Figure 3 denote the magnetograms of active regions that were CME productive in the ±2-day window, and the diamonds are for the magnetograms of active regions that produced no CMEs in the window. The first of the 2 × 2 contingency tables in Table 3 assesses the correlation of L_{SS} with CME productivity in our data set. As can be seen in Figure 3 (and in Table 1), in 15 of the 17 magnetograms, the active region either had an L_{SS} at or above threshold and was CME-productive or had an L_{SS} below threshold and produced no CMEs in the window. One magnetogram of a CME-productive active region had an L_{SS} below threshold, and one magnetogram of a non-CME-productive active region had an L_{SS} above threshold. Thus in our data set, with our choice of L_{SS} threshold for deciding whether an active region should be expected to be CME productive, the correlation of L_{SS} with CME productivity is statistically significant, having a confidence level of 99.7% and a success rate of 88%.

[21] For each of the three $|\nabla B_{||}|$ thresholds, the 2 × 2 contingency table for the correlation of L_{SG} with CME productivity is given in Table 3, and the resulting confidence level and success rate of the correlation are listed in Table 3 and given in the upper left corner of the corresponding correlation plot in Figure 3. As can be verified from Table 1, for L_{SG} defined by $|\nabla B_{||}|$ >50 G/Mm, there were only two failures out of 17 trials: one magnetogram of a CME-productive active region had an L_{SG} below threshold, and one magnetogram of a non-CME-productive active region had an L_{SG} at threshold. Decreasing the L_{SG}-defining $|\nabla B_{||}|$ threshold from 50 G/Mm to 25 G/Mm resulted in the number of failures increasing by one step (from 2 to 4). Increasing the L_{SG}-defining $|\nabla B_{||}|$ threshold from 50 to 100 G/Mm resulted in the number of failures decreasing by one step (from 2 to 0). (Because the $L_{SG} \geq$ threshold row and the CME-producing column in the 2 × 2 contingency table each always totals 8, while the $L_{SG} <$ threshold row and the not CME-producing column each always total 9, when the population of one of the two "failure" quadrants increases or decreases by 1, the population of the other "failure" quadrant must also increase or decrease by 1.) We consider a single step up or down in the failure rate to be an insignificant difference. So we find that in our data set, for L_{SG}-defining $|\nabla B_{||}|$ thresholds in the vicinity of 50 G/Mm, L_{SG} is statistically significantly correlated with CME productivity (confidence level >95%), and L_{SG} is about as strongly correlated with CME productivity as is L_{SS} (confidence level ∼99.7%, success rate ∼88%).

4. Conclusion

[22] In our sample of 17 vector magnetograms of 12 bipolar active regions we have measured in each magnetogram the length L_{SS} of strong magnetic shear on the main neutral line and the length L_{SG} of strong gradient in the line-of-sight magnetic field ($|\nabla B_{||}|$ above some threshold) on the main neutral line. In our previous investigation of L_{SS} measured from these vector magnetograms [*Falconer et al.*, 2002] we have shown that L_{SS} is a measure of the overall nonpotentiality of a bipolar active region and that L_{SS} is strongly enough correlated with active region CME productivity that it would be useful in CME forecasting if it were continuously available for each active region on the central face of the Sun. In the present work we have found that for a $|\nabla B_{||}|$ threshold in the vicinity of 50 G/Mm, (1) L_{SG} is

statistically significantly correlated with L_{SS}, (2) L_{SG} is statistically significantly correlated with active region CME productivity, and (3) the correlation of L_{SG} with CME productivity is about as strong as the correlation of L_{SS} with CME productivity. We therefore conclude that L_{SG} is a measure of active region nonpotentiality that can be measured from a line-of-sight magnetogram and that is strongly enough correlated with active region CME productivity that it should be useful in operational CME forecasting.

[23] Our sample of 17 vector magnetograms is large enough to establish the above results but not large enough to determine whether the L_{SG}-defining $|\nabla B_{\|}|$ threshold that gives the strongest correlation of L_{SG} with L_{SS}, or that gives the strongest correlation of L_{SG} with CME productivity, is 50 G/Mm, somewhat larger or somewhat smaller. Determination of this will require a sample of at least 50–100 magnetograms. For examining the correlation of L_{SG} with L_{SS} these magnetograms have to be vector magnetograms. The archive of MSFC vector magnetograms is ample to yield a sample of this size, and we are presently expanding our sample.

[24] Although the optimum $|\nabla B_{\|}|$ threshold for determining L_{SG} may be somewhat above or below 50 G/Mm, it is clear from our present sample that L_{SG} is a viable proxy for L_{SS} that can be measured from a line-of-sight magnetogram, and as such should be of practical use in CME forecasting. In addition, like L_{SS}, L_{SG} can be directly generalized to serve as a measure of the overall nonpotentiality of multibipolar active regions: The generalized L_{SG} is the total length of strong magnetic gradient on all neutral lines in an active region rather than just on the main neutral line. Furthermore, L_{SG} opens the years-long record of 1.5-hour cadence full disk line-of-sight magnetograms from SOHO/MDI to measurement of the growth and decay of the nonpotentiality of whole active regions for investigation of (1) the origin and evolution of large-scale magnetic shear and twist in active regions and (2) the dependence of active region CME productivity on the direction and rate of change of active region nonpotentiality.

[25] **Acknowledgments.** The research reported in this paper was supported by funding from NSF's Division of Atmospheric Sciences through its Space Weather program and its SHINE program and by funding from NASA's Office of Space Science through the Living With a Star program and the Solar Physics Supporting Research and Technology program of its Sun-Earth Connection Division.

[26] Shadia Rifai Habbal thanks Bernard V. Jackson and another referee for their assistance in evaluating this paper.

References

Aulanier, G., E. E. DeLuca, S. K. Antiochos, R. A. McMullen, and L. Golub, The topology and evolution of the Bastille Day flare, *Astrophys. J.*, *540*, 1126–1142, 2000.

Canfield, R. C., H. S. Hudson, and D. E. McKenzie, Sigmoidal morphology and eruptive solar activity, *Geophys. Res. Lett.*, *26*, 627–630, 1999.

Everitt, B. S., *The Analysis of Contingency Tables*, Chapman and Hall, New York, 1977.

Falconer, D. A., A correlation between length of strong-shear neutral lines and total X-ray brightness in active regions, *Sol. Phys.*, *176*, 123–126, 1997.

Falconer, D. A., A prospective method for predicting coronal mass ejections from vector magnetograms, *J. Geophys. Res.*, *106*(A11), 25,185–25,190, 2001.

Falconer, D. A., R. L. Moore, J. G. Porter, G. A. Gary, and T. Shimizu, Neutral-line magnetic shear and enhanced coronal heating in solar active regions, *Astrophys. J.*, *482*, 519–534, 1997.

Falconer, D. A., R. L. Moore, and G. A. Gary, Correlation of the coronal mass ejection productivity of solar active regions with measures of their global nonpotentiality from vector magnetograms: Baseline results, *Astrophys. J.*, *569*, 1016–1025, 2002.

Gary, G. A., R. L. Moore, M. J. Hagyard, and B. M. Haisch, Nonpotential features observed in the magnetic field of an active region, *Astrophys. J.*, *314*, 782–794, 1987.

Hagyard, M. J., N. P. Cumings, E. A. West, and J. E. Smith, The MSFC vector magnetograph, *Sol. Phys.*, *80*, 33–51, 1982.

Hathaway, D., et al., Solar dynamics observatory: Report of the science definition team, NASA, Washington, D. C., 2001.

Machado, M. E., R. L. Moore, A. M. Hernandez, M. G. Rovira, M. J. Hagyard, and J. B. Smith Jr., The observed characteristics of flare energy release. I. Magnetic structure at the energy release site, *Astrophys. J.*, *326*, 425–450, 1988.

MacQueen, R. M., and R. R. Fisher, The kinematics of solar inner coronal transients, *Sol. Phys.*, *89*, 89–102, 1983.

Moore, R., Solar prominence eruption, in *Encyclopedia of Astronomy and Astrophysics*, edited by P. Murdin, pp. 2691–2695, Inst. of Phys. Publ., Bristol, UK, 2001.

Moore, R., and D. Rabin, Sunspots, *Ann. Rev. Astron. Astrophys.*, *23*, 239–266, 1985.

Moore, R. L., Evidence that magnetic energy shedding in solar filament eruptions is the drive in accompanying flares and coronal mass ejections, *Astrophys. J.*, *324*, 1132–1137, 1988.

Moore, R. L., and B. J. LaBonte, The filament eruption in the 3B flare of July 29, 1973: Onset and magnetic field configuration, in *Solar and Interplanetary Dynamics*, edited by M. Dryer and E. Tandberg-Hanssen, pp. 207–210, D. Reidel, Norwell, Mass., 1980.

Moore, R. L., M. J. Hagyard, and J. M. Davis, Flare research with the NASA/MSFC vector magnetograph: Observed characteristics of sheared magnetic fields that produce flares, *Sol. Phys.*, *113*, 347–352, 1987.

Moore, R. L., B. Schmeider, D. H. Hathaway, and T. D. Tarbell, 3-D magnetic field configuration late in a large two-ribbon flare, *Sol. Phys.*, *176*, 153–169, 1997.

Moore, R. L., D. A. Falconer, J. G. Porter, and S. T. Suess, On heating the Sun's corona by magnetic explosions: Feasibility in active regions and prospects for quiet regions and coronal holes, *Astrophys. J.*, *526*, 505–522, 1999.

Moore, R. L., A. C. Sterling, H. S. Hudson, and J. R. Lemen, Onset of the magnetic explosion in solar flares and coronal mass ejections, *Astrophys. J.*, *552*, 848–883, 2001.

Reames, D. V., SEPs: Space weather hazard in interplanetary space, in *Space Weather*, *Geophys. Monogr. Ser.*, vol. 125, edited by P. Song, H. J. Singer, and G. L. Siscoe, pp. 101–107, AGU, Washington, D. C., 2001.

Rust, D. M., et al., Mass ejections, in *Solar Flares: A Monograph from Skylab Solar Workshop II*, edited by P. A. Sturrock, pp. 273–339, Colo. Assoc. Univ. Press, Boulder, Colo., 1980.

Scherrer, P. H., et al., The solar oscillations investigation-Michelson Doppler imager, *Sol. Phys.*, *162*, 129–188, 1995.

Sterling, A. C., and R. L. Moore, Internal and external reconnection in a series of homologous solar flares, *J. Geophys. Res.*, *106*(A11), 25,227–25,238, 2001.

Suess, S. T., and B. T. Tsurutani (Eds.), *From the Sun: Auroras, Magnetic Storms, Solar Flares, Cosmic Rays*, AGU, Washington, D. C., 1998.

Webb, D. F., The solar sources of coronal mass ejections, in *Eruptive Solar Flares*, edited by Z. Svestka, B. V. Jackson, and M. E. Machado, pp. 234–247, Springer-Verlag, New York, 1992.

West, E. A., M. J. Hagyard, G. A. Gary, J. E. Smith, M. Adams, and R. Cloyd, Development of a NEW vector magnetograph at Marshall Space Flight Center (MSFC), *Proc. SPIE*, *4441*, 270–280, 2002.

Zirin, H., *Astrophysics of the Sun*, Cambridge Univ. Press, New York, 1988.

Zirin, H., and M. A. Liggett, Delta sunspots and great flares, *Sol. Phys.*, *113*, 267–283, 1987.

D. A. Falconer, G. A. Gary, and R. L. Moore, Marshall Space Flight Center, SD 50, Huntsville, AL 35812, USA. (david.falconer@msfc.nasa.gov)